

Local Scale Equivariance with Latent Deep Equilibrium Canonicalizer

Md Ashiqur Rahman¹ Chiao-An Yang¹ Michael N. Cheng¹ Lim Jun Hao²

Jeremiah Jiang² Teck-Yian Lim² Raymond A. Yeh¹

¹Department of Computer Science, Purdue University ²DSO National Laboratories

Abstract

Scale variation is a fundamental challenge in computer vision. Objects of the same class can have different sizes, and their perceived size is further affected by the distance from the camera. These variations are local to the objects, *i.e.*, different object sizes may change differently within the same image. To effectively handle scale variations, we present a deep equilibrium canonicalizer (DEC) to improve the local scale equivariance of a model. DEC can be easily incorporated into existing network architectures and can be adapted to a pre-trained model. Notably, we show that on the competitive ImageNet benchmark, DEC improves both model performance and local scale consistency across four popular pre-trained deep-nets, *e.g.*, ViT, DeiT, Swin, and BEiT. Our code is available at <https://github.com/ashiq24/local-scale-equivariance>.

1. Introduction

The perceived scale of an object in images varies due to multiple factors. First, intrinsic factors such as the object’s physical dimensions cause variations in the apparent size, *e.g.*, individuals may differ in height. Second, extrinsic factors such as camera zoom and the object’s distance to the camera further affect the observed scale, even for the same object. How to effectively handle and represent this scale variation has been a fundamental question in computer vision. Inspired by human vision, which uses a hierarchy of scales for perception [42], earlier works adopted image pyramids [1, 12] and variants [34, 55, 65] to extract features at different image resolutions [21, 31, 39, 40].

In deep learning, ideas similar to image pyramids have been introduced [14, 20, 24, 76] and studied under the broad area of scale invariance/equivariance [48, 56, 57, 67]. These works aim to design specialized deep-nets such that the network’s output is transformed in a predefined way when the input image undergoes scale changes (image resizing). Mathematically, equivariance is formalized as equality statements over groups; see Sec. 3 for a review. A typical approach is to design a group equivariant architecture [15] by modifying the

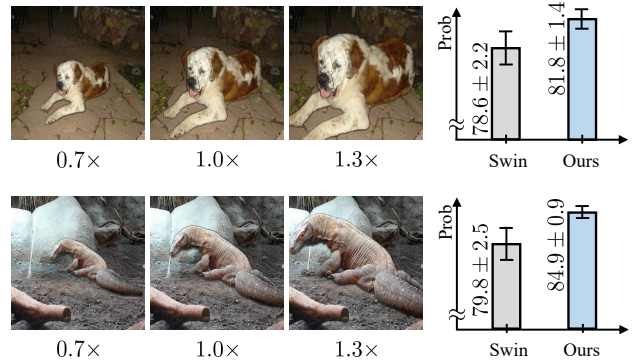


Figure 1. Local scaling resizes different parts of an image independently, *e.g.*, the dog is scaled while the background remains unchanged. For the Swin model [38], we show the distribution of predicted probabilities for the object class across a set of locally scaled images. Observe that the predicted probabilities are not stable, indicating that the Swin model is not consistent across local scaling. We introduce Deep Equilibrium Canonicalizer (Ours) to address this issue.

filter operations. Note, we use the term “equivariance” in the strict mathematical sense of the *exact equality statement*. We will use the term “consistency” to mean an approximation of equivariance, *i.e.*, without the mathematical guarantees.

While scale equivariance has been well studied, these works all focused on *global scaling*, *i.e.*, changes in image resolution. Differently, we are interested in *local scaling*, *e.g.*, the resizing of each part of an input image differently (at a fixed resolution), which more closely matches the scaling of objects in the real world. See illustration in Fig. 1. Ideally, we aim to design deep-nets that are local scale equivariant. However, real-world local scaling does not form a group as the operation is not invertible, *e.g.*, when two objects change size and occlude each other. To address this, we propose an approximation of the real-world local scaling operation, namely monotone scaling, which we will show to be a group.

Our approach to making a deep-net monotone scale equivariant is based on the framework of canonicalization [44, 46]. Briefly, a canonicalizer transforms an input into a “standard” (canonical) form so that the deep network can extract invariant features. A canonicalizer can be modeled as finding a stationary point of a learned energy function with respect to

the transformation (group) and then using that point as the “standard”. Instead of this optimization approach, we propose to utilize a deep equilibrium model [4] for directly predicting this point, *i.e.*, amortized optimization [2]. We name our approach the Deep Equilibrium Canonicalizer (DEC). We then incorporate DEC into the latent space of existing deep-net architectures to improve the local scale consistency.

To evaluate local scale consistency, we first conduct experiments on semantic segmentation using synthetic data where we can control the scale variation. We create a dataset of realistic renderings using physical simulation based on the Google Scan Objects [19]. Next, we consider the task of image classification. Inspired by the MNIST-scale dataset used in prior works [29, 48, 57], we create a dataset of locally scaled MNIST images where each image contains multiple MNIST digits, resized to a different scale. Finally, we evaluate a locally scaled version of ImageNet [17]. Overall, our proposed DEC, when incorporated into existing models, achieves a higher performance metric and further improves the local scale consistency over the existing base model.

Our main contributions are as follows:

- Motivated by local scaling in the real world, we propose to study how to design deep-nets that are equivariant to monotone scaling.
- We propose DEC, a novel latent canonicalization approach based on deep equilibrium models, which can be easily incorporated into existing deep-net architectures.
- We demonstrate that the proposed DEC improves model performance and local scale consistency on two vision tasks, notably, the competitive benchmark of ImageNet across four different ViT architectures.

2. Related Works

Scale consistency has a long history in computer vision. Early works focus on developing methods that are invariant to scaling [40, 66] with techniques such as Laplacian image pyramids [11, 55] or wavelet analysis [62]. Later works aim to improve scale consistency by learning transformations applied either to the input images or directly to convolutional filters [16, 27, 52, 59] or by directly learning local/global scale estimation [8, 33]. More recently, variants of vision transformer models have been proposed to tackle scale consistency, *e.g.*, incorporating the structure of image pyramids [22, 60]. While some of these works use the term invariance/equivariance, these approaches generally do not achieve the equality condition on a group, *i.e.*, they are not guaranteed to be scale equivariant in the strict sense. In the equivariant literature, there is a line of work studying global scaling [48, 56, 57, 67, 69] through designing specialized architecture based on group theory.

Group equivariant models. Designing group equivariant architectures has been explored due to their strong theoretical guarantees and robustness [13, 15, 41, 47, 72]. Their

development has been extended to incorporate equivariance in rotation [63], shift [54, 75], permutation [23, 35, 36, 51, 70, 71, 74], and sampling [49, 53, 68]. Global scale equivariant architectures are primarily constructed by integrating over the scale space of images [67], through the use of steerable filter [56] or applying spectral-domain operations for anti-aliasing [48]. However, the current literature lacks equivariant methods for local scaling (as it does not form a group) and only handles the global scaling operations.

Equivariant via canonicalization. With the rise of pre-trained models, there is growing interest in adapting existing models to be equivariant rather than developing entirely new equivariant architectures. This has led to the area of group equivariant adaptation, which primarily aims to “standardize” the input through the use of a canonicalization module [44, 46] or by averaging over the group elements to achieve more stable output [9, 10]. However, these methods target discrete symmetry groups with a few parameters, *e.g.*, the 2D rotation group ($SO(2)$) characterized by a single parameter. These approaches are limited when the size and dimensionality of the transformation group increases.

Deep Equilibrium Models (DEQs) are a class of implicit neural networks that compute their outputs by solving for the fixed point of a parameterized transformation [4, 5]. Unlike traditional deep networks with a predefined number of layers, DEQs effectively model an infinitely deep, weight-tied recurrent network, making them highly parameter-efficient. These models have been applied successfully in various applications, including optical flow estimation [6] and video landmark detection [43]. In this work, we found DEQs to be a suitable architecture for modeling a canonicalizer for adapting deep-nets to be equivariant.

3. Preliminaries

We provide a review of the definition of equivariance and invariance. For readability, we describe these concepts using one-dimensional functions. Next, we review the canonicalization framework for achieving equivariant models.

Global scaling operation. The global scaling operation \mathbf{R}_a on a 1D function $f \in \mathcal{U}$, where $\mathcal{U} \triangleq \{f : [0, 1] \rightarrow \mathbb{R}\}$, is defined as

$$\mathbf{R}_a[f](x) = f(a^{-1}x), \quad (1)$$

where $a \in \mathbb{R}^+$ is the scaling factor. Specifically, \mathbf{R}_a with $a > 1$ is an upscaling operation, and $a < 1$ is a downscaling operation.

Group and equivariance. A group is a mathematical structure consisting of a set G , which captures the structure of symmetry transformations. The action of a group element $g \in G$ on any function $f \in \mathcal{U}$ is represented by a transformation $\mathbf{T}(\cdot; g)$ as

$$\mathbf{T}(f; g) = f(g^{-1} \cdot x), \quad (2)$$

where $g^{-1} \cdot x$ denotes the transformation of x by the inverse element g^{-1} . In other words, the function is evaluated at the transformed input $g^{-1} \cdot x$. Here, g acts as the parameter of the transformation \mathbf{T} . By definition, the transformation needs to satisfy the invertibility condition, $\mathbf{T}^{-1}(f; g) = \mathbf{T}(f; g^{-1})$, for any group element g .

Next, a neural network \mathcal{M} is said to be *equivariant* with respect to the group G if \mathcal{M} commutes with the action of G , *i.e.*, satisfying the following equality condition

$$\mathcal{M}(\mathbf{T}(f; g)) = \mathbf{T}(\mathcal{M}(f); g). \quad (3)$$

That is, transforming the input similarly transforms the output. The neural network \mathcal{M} is *invariant* if

$$\mathcal{M}(\mathbf{T}(f; g)) = \mathcal{M}(f), \quad (4)$$

which means transforming the input by a group element $g \in G$ does not change the output.

Learned canonicalization function. A canonicalization function can modify \mathcal{M} , ensuring the resulting $\tilde{\mathcal{M}}$ is equivariant. The canonicalization function $h : \mathcal{U} \rightarrow G$ is designed to be equivariant with respect to the group G , *i.e.*,

$$h(\mathbf{T}(f; g)) = g \cdot h(f), \forall g \in G, \quad (5)$$

where $g \cdot h(f)$ denotes a group product. Using this canonicalization function, the adapted model $\tilde{\mathcal{M}}$ is defined as:

$$\tilde{\mathcal{M}}(f) \triangleq \mathbf{T}(\mathcal{M}(\mathbf{T}^{-1}(f; \tilde{g})); \tilde{g}), \quad (6)$$

where $\tilde{g} \triangleq h(f)$. In particular, the canonicalization module maps all possible transformed versions of a function f to a canonical input represented as $\mathbf{T}^{-1}(f; \tilde{g})$.

The canonicalization function h can be modeled directly by group equivariant networks [28, 44]. In the absence of an equivariant model, an alternative approach is to formulate the canonicalizer as an optimization problem [41, 46]

$$h(f) \triangleq \arg \min_{g \in G} E(\mathbf{T}^{-1}(f; g)). \quad (7)$$

Here, $E : \mathcal{U} \rightarrow \mathbb{R}$ is a learnable *energy function*, *e.g.*, modeled with a neural network.

4. Latent Deep Equilibrium Canonicalizer

In Sec. 4.1, we formulate the monotone scaling group to approximate the local scaling transformation. Next, we introduce our DEC module in Sec. 4.2 for effective canonicalization on a given module. Lastly, we propose latent canonicalization for adapting pretrained models in Sec. 4.3.

4.1. Local Scaling

In contrast to the global scaling (Eq. (1)), scalings in a real-world image are often local. As shown in Fig. 1, different

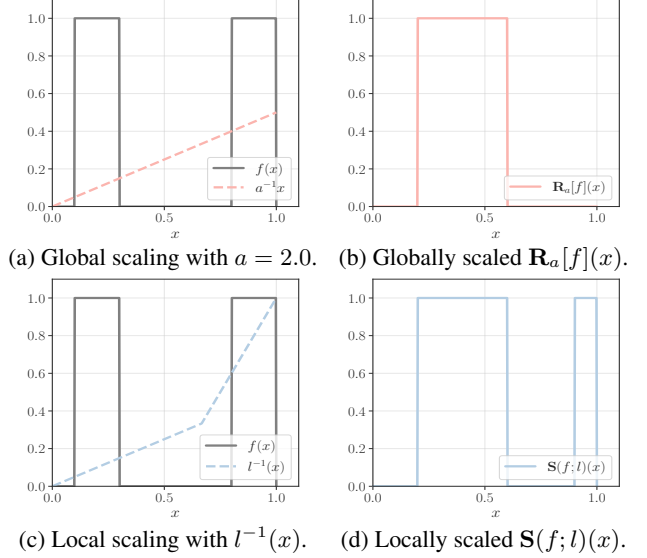


Figure 2. **Comparison of global and local scaling.** (a-b) In global scaling, all locations of $f(x)$ are scaled by a constant factor. (c-d) In local scaling, each segment of $f(x)$ is scaled differently.

regions in an image have different scaling factors. To approximate such transformations, we propose monotone scaling operations. For readability, the idea is first discussed in 1D and then extended to 2D for images.

Monotone scaling operation. To apply different scaling factors at different parts of the domain, we propose to perform the scaling by a function $l : [0, 1] \rightarrow [0, 1]$. A monotone scaling is defined as follows

$$\mathbf{S}(f; l)(x) \triangleq f(l^{-1}(x)), \quad (8)$$

where l^{-1} is the inverse function of l and the local scaling factor at t is $\frac{dl}{dt}$. To preserve the smoothness and invertibility of this transformation, we restrict the functions l to be strictly monotonic, increasing, and continuous. In Fig. 2, we provide a comparison between the global and our local scaling operation.

Monotone scaling group. Denote the set of all continuous and strictly monotonic increasing functions l as L . The set L forms a group structure, where the group product “.” is represented as the function composition as

$$(l_1 \cdot l_2)(x) = (l_1 \circ l_2)(x) = l_1(l_2(x)). \quad (9)$$

We formally state this in Lemma 1.

Lemma 1. *The set of all continuous strictly monotonic increasing functions L is a group under the binary operation of function composition.*

Proof. We provide the proof of this lemma in Sec. A3.1. \square

Lemma 1 states that the proposed monotone scaling operation forms a group. Hence, we can formally define equiv-

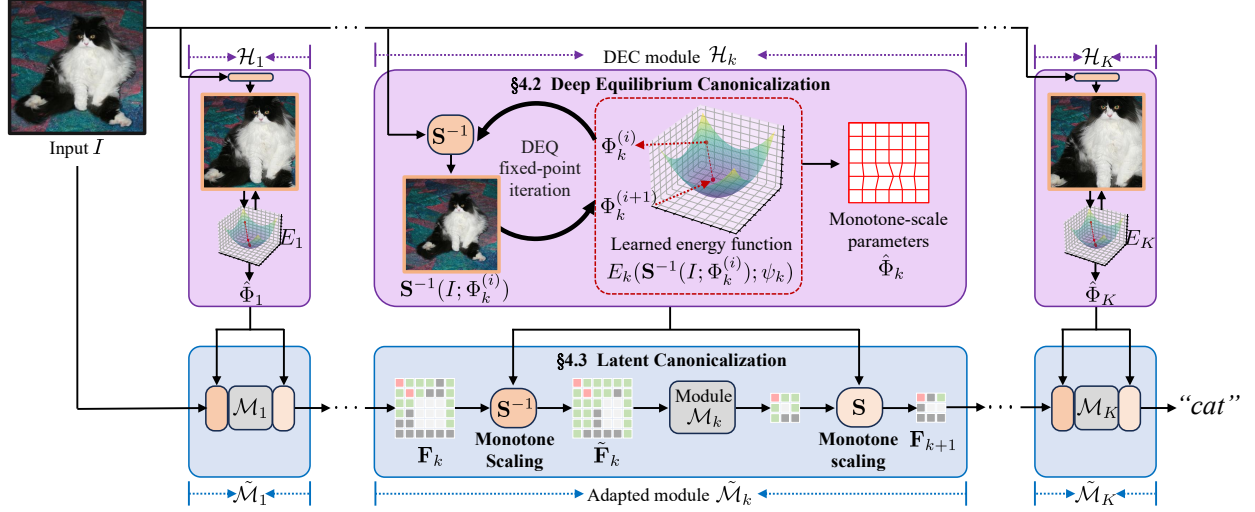


Figure 3. **Illustration of the proposed method.** We formulate a neural network as a sequence of modules $\{\tilde{\mathcal{M}}_k\}_{k=1:K}$. We perform latent canonicalization (see Sec. 4.3) on the latent feature \mathbf{F}_k of each intermediate module. The monotone scaling in the latent canonicalization, *i.e.*, \mathbf{S}^{-1} and \mathbf{S} , are controlled by the parameters Φ_k found by our DEC module \mathcal{H}_k (see 4.2). Each \mathcal{H}_k finds the optimal $\hat{\Phi}_k$ through an iterative fixed-point solver on the energy function E_k until convergence.

ariance of w.r.t. the monotone scaling group as

$$\text{Equivariance: } \mathcal{M}(\mathbf{S}(I; l)) = \mathbf{S}(\mathcal{M}(I); l) \quad (10)$$

and invariance as

$$\text{Invariance: } \mathcal{M}(\mathbf{S}(I; l)) = \mathcal{M}(I). \quad (11)$$

Parameterization of l . The family of possible functions in l is very flexible. For simplicity, we consider a parametric l in the form of a piecewise linear function where the domain $[0, 1]$ is discretized uniformly into N discrete points as $\{x_0 = 0, x_1, \dots, x_N = 1\}$. In this case, l has the form

$$l_\Phi(x) = \phi_{n-1} + \frac{\phi_n - \phi_{n-1}}{x_n - x_{n-1}} \times (x - x_{n-1}), \quad (12)$$

when $\Phi = \{\phi_0, \dots, \phi_N\}$ are the parameters. We impose the restriction $\phi_{n-1} < \phi_n$ to make the l monotonic increase and further we impose $\phi_0 = 0$ and $\phi_N = 1$ to make the function bijective. For the ease of notation, we denote the monotone scaling by l_Φ as $\mathbf{S}(f; \Phi)$, by dropping the l , *i.e.*, $\mathbf{S}(f; \Phi) \triangleq \mathbf{S}(f; l_\Phi)$.

A similar piecewise linear l can be constructed for monotone scaling operation to images $I : [0, 1]^2 \rightarrow \mathbb{R}$ by extending the definition of l to the 2D domain, *i.e.*,

$$\mathbf{S}(I; l)(x, y) = I(l^{-1}(x, y)), \quad (13)$$

where $l : [0, 1]^2 \rightarrow [0, 1]^2$. We illustrate this monotone scaling operation in Fig. 4. More details are provided in Appendix A2.2. With the parameterization and monotone scaling group defined, we now discuss how to design an effective canonicalizer for this group.

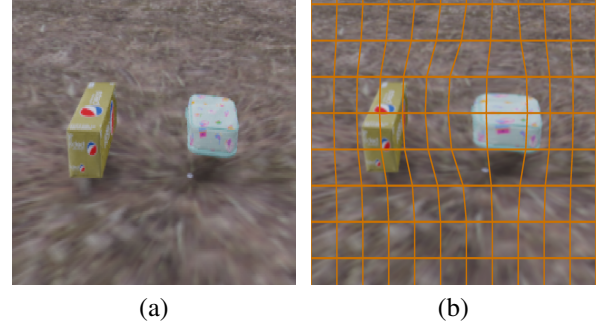


Figure 4. Scaling by monotone function $l : [0, 1]^2 \rightarrow [0, 1]^2$. (a) The original image. (b) Scaled image. The warped grid visualizes the effect of the monotone scaling operation.

4.2. Deep Equilibrium Canonicalization (DEC)

As reviewed in Sec. 3, one approach to formulate a canonicalizer is by solving for a stationary point, *e.g.*, a minimum of an energy function with respect to the group elements in Eq. (7). However, solving Eq. (7) per example and training it end-to-end is slow and memory intensive. Instead, we propose to leverage the idea of amortized optimization [2], *i.e.*, we learn a model to directly predict the solution. In our case, we choose this prediction model to be a Deep equilibrium model to be used as the canonicalizer.

Deep equilibrium model (DEQ) is a type of implicit neural network where the output is expressed as the fixed/stationary point of a learnable non-linear transformation \mathcal{H} , *i.e.*,

$$\hat{\mathbf{z}} = \mathcal{H}(\hat{\mathbf{z}}; I, \psi), \quad (14)$$

where \mathcal{H} is the non-linear transformation with parameter ψ and $\hat{\mathbf{z}}$ is the equilibrium hidden state. The equilibrium can

be calculated implicitly by solving the equilibrium condition

$$\mathbf{z} - \mathcal{H}(\mathbf{z}; I, \psi) = \mathbf{0} \quad (15)$$

DEQ can be trained from end to end like any other differentiable module, where the backpropagation can be efficiently computed using implicit differentiation.

DEC module. We propose to formulate the canonicalization module using a DEQ. That is, we model the optimization in Eq. (7) as a fixed point of a non-linear system \mathcal{H} . Specifically, we treat Φ as the hidden state \mathbf{z} described in Eq. (14) and define the update as

$$\mathcal{H}(\Phi^{(i+1)}; I, \psi) \triangleq \Phi^{(i)} - \nabla_{\Phi^{(i)}} E(\mathbf{S}^{-1}(I; \Phi^{(i)}); \psi). \quad (16)$$

As shown in Fig. 3, our DEC finds the optimal monotone-scale parameters $\hat{\Phi}$ via DEQ fixed-point iteration to canonicalize the input I .

Claim 1. *The optimal monotone-scale parameter, $\hat{\Phi}$, of energy function E obtained via gradient descent is a fixed point of \mathcal{H} .*

Proof. We assume that both DEQ iteration and the gradient descent optimization (Eq. (7)) start from the same initialization $\Phi^{(0)}$. Let Φ^\dagger be a fixed point of \mathcal{H} for the input I . Therefore it satisfies

$$\Phi^\dagger = \mathcal{H}(\Phi^\dagger; I, \psi) \quad (17)$$

$$\Rightarrow \Phi^\dagger = \hat{\Phi}^\dagger - \nabla_{\hat{\Phi}^\dagger} E(\mathbf{S}^{-1}(I; \Phi^\dagger); \psi) \quad (18)$$

$$\Rightarrow \nabla_{\Phi^\dagger} E(\mathbf{S}^{-1}(I; \Phi^\dagger); \psi) = \mathbf{0} \quad (19)$$

This implies that the gradient of the energy function E , $\nabla_{\Phi} E$, evaluated at point Φ^\dagger is $\mathbf{0}$. Therefore, Φ^\dagger corresponds to some stationary point. Consequently, Φ^\dagger corresponds to a local minimum and thus represents the optimal parameter returned by the gradient descent optimization in Eq. (7). \square

The main insight of our canonicalizer design is that, instead of modeling \mathcal{H} in terms of the gradient of E , we directly model \mathcal{H} using a neural network with learnable parameters ψ and use it as the canonicalization module. Given an image I and monotone-scale parameter $\Phi^{(i)}$ at step i , \mathcal{H} predict the next-step parameter $\Phi^{(i+1)}$ based on inversely scaled image $\mathbf{S}^{-1}(I, \Phi^{(i)})$. This process is repeated iteratively until convergence to the equilibrium point. The equilibrium point $\hat{\Phi}$ can be determined by using Anderson acceleration [3].

With our modeled canonicalizer defined, the remaining question is how to incorporate it into an existing deep-net.

4.3. Latent Canonicalization

Typically, canonicalization [41, 44, 46] methods apply the canonicalizer at the input of the deep-net. This approach is effective when the transformation of interest is fully represented by the group actions, such as 2D rotation. However, recall that monotone scaling is only an approximation of the

real-world local scaling. Therefore, we propose to canonicalize the latent features of an existing network. We demonstrate the process of latent canonicalization in Fig. 3. This is motivated by the hypothesis that the inductive bias of monotone scale equivariant features could better approximate an overall local scale equivariant deep-net.

Canonicalizer on the latent features. A deep-net \mathcal{M} can be viewed as a composition of multiple layers, *i.e.*,

$$\mathcal{M}(I) = \mathcal{M}_K \circ \mathcal{M}_{K-1} \circ \dots \circ \mathcal{M}_1(I). \quad (20)$$

Using this notation, we denote the latent feature maps $\mathbf{F}_{k+1} \triangleq \mathcal{M}_k(\mathbf{F}_k)$ where the input feature is the image, *i.e.*, $\mathbf{F}_1 = I$. For each layer \mathcal{M}_k , we use canonicalization to adapt it to $\tilde{\mathcal{M}}_k$ following Eq. (6). Our overall adapted model with equivariance guarantee is a composition of all adapted modules, *i.e.* $\tilde{\mathcal{M}} = \tilde{\mathcal{M}}_K \dots \circ \tilde{\mathcal{M}}_0$.

For monotone scale equivariance, we define each adapted module $\tilde{\mathcal{M}}_k$ as follows:

$$\tilde{\mathcal{M}}_k^{\text{Eq}}(\mathbf{F}_k) = \mathbf{S}(\mathcal{M}_k(\tilde{\mathbf{F}}_k); \Phi_k), \quad (21)$$

where $\tilde{\mathbf{F}}_k = \mathbf{S}^{-1}(\mathbf{F}_k; \Phi_k)$. That is, we first apply monotone scaling \mathbf{S}^{-1} to each input feature of each layer, *i.e.*, \mathbf{F}_k , and subsequently apply its inverse \mathbf{S} to the output of \mathcal{M}_k . This ensures that the latent feature is equivariant to monotone scaling. Similarly, for monotone scale invariance, we define the adapted modules as

$$\tilde{\mathcal{M}}_k^{\text{Inv}}(\mathbf{F}_k) = \mathcal{M}_k(\tilde{\mathbf{F}}_k). \quad (22)$$

5. Experiments

For evaluation, we aim to benchmark the local scale consistency of existing architectures and verify that the proposed DEC can improve consistency while maintaining model performance. To accurately measure the local scale consistency, we create datasets of locally scaled images where we know the underlying local scale transformation applied to each image. Specifically, we considered semantic segmentation on a dataset based on the Google Scan Objects [19] and image classification using the MNIST [32] dataset and the ImageNet [17] dataset. The implementation details are in the Appendix A1. More results are provided in the Appendix A5.

5.1. Semantic Segmentation

Dataset setup. For evaluating equivariance, we construct a locally scaled segmentation dataset by simulating real-world objects' scale variations. To have precise control over the variations, we render objects from Google Scanned Objects [19] on a randomly selected background in HDRI Haven [73]. For each image, we place two 3D objects and extract the ground-truth mask.

To introduce the local scaling effects, we vary the relative distance of each object from the camera and enable

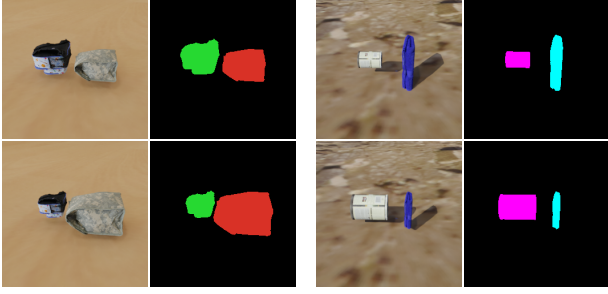


Figure 5. **Samples from locally scaled object segmentation dataset.** Each object in an image is scaled independently.

Method	ViT [18]		Swin [38]		DINOv2 [45]	
	mIoU \uparrow	EquE \downarrow	mIoU \uparrow	EquE \downarrow	mIoU \uparrow	EquE \downarrow
<i>Aug</i>	82.18	0.054	86.65	0.036	76.63	0.061
<i>Canon</i>	79.37	0.062	83.94	0.050	76.94	0.064
<i>AugL</i>	82.35	0.054	87.63	0.037	79.05	0.058
Ours	83.12	0.052	88.56	0.035	80.86	0.055

Table 1. **Results on local scale equivariance.** For each method, we report the mIoU(%) and EquE across 3 architectures.

independent scale changes for each object while keeping the background fixed. The dataset includes 100 distinct objects; see Fig. 5 for examples. We use 6,000 images for training and 2,000 for testing with an image resolution of 256×256 .

Evaluation metric. To measure performance, we report the mean intersection over union (mIoU). To measure consistency, we propose monotone scale equivariance error (EquE) on the predicted masked, defined as

$$\frac{1}{|\mathcal{D}|} \sum_{I \in \mathcal{D}} \mathbb{E}_{\Phi \sim \Omega} \|\mathcal{S}(\mathcal{M}(I); \Phi) - \mathcal{M}(\mathcal{S}(I; \Phi))\|_2^2 \quad (23)$$

over a dataset \mathcal{D} and Ω denotes a uniform distribution over all possible monotone scale parameters.

Intuitively, EquE can be thought of as a *soft* definition, in the ℓ_2 sense, of the monotone scale equivariance in Eq. (10). That is, an equivariant model will achieve an EquE of zero.

Baselines. We consider the following alternative methods to encourage local scale consistency into a model:

- *Aug*: We train the architecture with random monotone scaling data augmentation on the training set. *Aug* also serves as the starting weights for DEC and the other baselines.
- *Canon*: We discretize the local scaling parameter and consider a set of 64 different parameters, including the identity transformation. We use a 3-layer CNN to model the energy function in Eq. (7).
- *AugL*: As one of the metrics is the equivariance error, we further fine-tune *Aug* by using EquE in Eq. (23) as part of the loss to encourage local scale equivariance.

The baselines and our DEC are applied to three deep-net architectures: ViT [18], Swin [38], and DINOv2 [45].

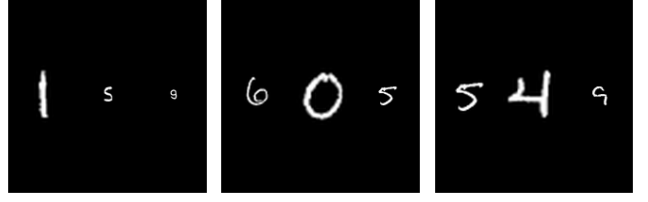


Figure 6. **Samples from locally scaled MNIST.** The task is to regress the number, *i.e.*, “159”, “605”, and “549” are the ground-truth for each of the images. In other words, an image classification task of 1000 classes; from 0 to 999.

Results. In Tab. 1, we compare our DEC with the equivariant adaptation baselines in semantic segmentation. We observe that ours achieves the highest mIoU and lowest EquE in all cases. Although *Aug* is effective in pursuing local scale equivariance, they are far from optimal. Comparison of *Aug* and ours shows that mere data augmentation with local scaling operations is not reliable enough to guarantee equivariance, nor does further guiding *Aug* with the Eq. (23) in *AugL*.

In contrast, *Canon* degrades the performance of *Aug* in most cases. That is, complete canonicalization on the input image only induces deterioration to the model. This shows the importance of canonicalization on latent features and replacing gradient optimization with our DEC, *i.e.*, solving a fixed-point equation iteratively.

Lastly, consistent improvements of ours on 3 distinct architectures demonstrate the generalizability of our model to different deep-nets. On average, ours outperforms the best baseline, *i.e.*, *AugL*, in mIoU by 1.17%.

5.2. Image Classification — MNIST

Dataset setup. Inspired by the MNIST-scale dataset from scale equivariance [29, 48, 57], we construct a locally scaled MNIST by creating 3-digit images from “000” to “999”. Each digit is randomly resized by a factor within $[0.4, 2.0]$, allowing for a scale variation of up to 5 times between different digits (see Fig. 6). The images have a resolution of 224×224 . This provides a suitable setup to test the local scale invariance, where the task is to predict the 1,000 number classes. As this task is relatively easy, we consider the more difficult setting with limited training data. The training set consists of 6,000 samples, while the test set contains 50,000 samples. The train/test images of the locally scaled dataset are sampled from the train/test split of the MNIST, respectively.

Evaluation Metric. We report the top-1 classification accuracy and the local scale invariance error

$$\text{InvE} \triangleq \frac{1}{|\mathcal{D}| |\mathcal{S}_I|} \sum_{I \in \mathcal{D}} \sum_{I_s \in \mathcal{S}_I} \|\mathcal{M}(I) - \mathcal{M}(I_s)\|_2^2. \quad (24)$$

Method	ResNet [25]		ViT [18]		DeiT [61]		Swin [38]		BEiT [7]		DINOv2 [45]	
	Acc \uparrow	InvE \downarrow	Acc \uparrow	InvE \downarrow	Acc \uparrow	InvE \downarrow	Acc \uparrow	InvE \downarrow	Acc \uparrow	InvE \downarrow	Acc \uparrow	InvE \downarrow
<i>Aug</i>	93.09 \pm 0.41	13.71 \pm 1.65	91.23 \pm 1.80	13.33 \pm 1.72	90.91 \pm 1.18	16.17 \pm 4.94	94.26 \pm 0.25	5.44 \pm 1.65	94.70 \pm 0.37	9.69 \pm 1.94	95.80 \pm 0.29	7.47 \pm 1.33
<i>Canon</i>	94.22 \pm 0.33	13.84 \pm 1.05	93.73 \pm 0.61	12.32 \pm 2.35	95.01 \pm 0.20	7.04 \pm 0.70	95.67 \pm 0.19	4.27 \pm 1.86	95.92 \pm 0.29	5.07 \pm 1.65	96.63 \pm 0.43	6.00 \pm 3.12
<i>InvL</i>	93.67 \pm 0.73	13.47 \pm 2.01	94.79 \pm 0.42	8.17 \pm 2.60	94.06 \pm 0.38	8.04 \pm 2.88	94.78 \pm 0.25	3.89 \pm 0.62	95.26 \pm 0.41	6.49 \pm 0.78	96.66 \pm 0.10	5.21 \pm 1.34
Ours	96.09 \pm 0.16	6.13 \pm 2.01	95.64 \pm 0.15	5.04 \pm 3.37	96.46 \pm 0.14	6.02 \pm 2.71	96.91 \pm 0.12	2.08 \pm 1.09	97.05 \pm 0.26	4.13 \pm 1.70	97.90 \pm 0.21	2.62 \pm 1.69

Table 2. **Results of local scale invariance on MNIST.** For each method, we report the Acc(%) and InvE(10^{-2}) across 6 architectures, with error bars computed over five runs.

Scale	[0.4, 1.0]	[1.0, 2.0]	[2.0, 3.0]	Overall
<i>Aug</i>	91.64	96.32	93.84	93.93 \pm 1.91
<i>Canon</i>	90.16	95.39	90.54	92.03 \pm 2.38
<i>InvL</i>	91.98	96.26	93.88	94.04 \pm 1.75
Ours	95.14	97.81	96.64	96.53 \pm 1.09

Table 3. **Per-scale results on MNIST.** We report the accuracy across various local scaling ranges using the Swin [38] architecture.

Here, \mathcal{S}_I consists of all variants of locally scaled I . Intuitively, InvE can be thought as a *soft* definition, in the ℓ_2 sense, of the local scale invariance in Eq. (11).

Baselines. We follow the same baselines of *Aug* and *Canon* from Sec. 5.1. Differently, as image classification should be invariant to local scaling, we instead have the baseline of *InvL*, which contains an additional loss of

$$\mathcal{L}_{\text{Inv}} = \mathbb{E}_{I \sim \mathcal{D}, \Phi \sim \Omega} \|\mathcal{M}(I) - \mathcal{M}(\mathcal{S}(I; \Phi))\|_2^2, \quad (25)$$

to encourage monotone scale invariance. We evaluate these baselines on commonly used image classification architectures, including ResNet [25], ViT [18], DeiT [61], Swin [38], BEiT [7], and DINOv2 [45].

Results. In Tab. 2, we compare our DEC with the baselines in image classification on MNIST. We have observations similar to the results in Tab. 1. *Aug* and *InvL* are not optimal while *AugL* degrades the performance of some architectures, e.g. ResNet, ViT, and Swin. Ours achieves the highest Acc and lowest InvE, no matter the architectures.

In particular, ours shows impressive results on local scale invariance and achieves a significant improvement in InvE compared to *Aug* and other baselines. Specifically, ours reduces InvE from 18.08 to 9.85 on ResNet and from 6.30 to 1.31 on DINOv2. This substantiates DEC’s ability to achieve local scaling invariance. On average, ours improves *Aug* on Acc by 4.10% and InvE by 8.91×10^{-2} . To further demonstrate the broad applicability of our model, we provide an additional comparison against hierarchical models [22, 60] in Sec. A5.1.

Analysis and ablation studies. In Tab. 3, we present the baseline results on Swin [38] across different local scale ranges. Specifically, we restrict the local scale range of each number digit in various scale brackets. We note that our method achieved higher accuracy in every scale range. Furthermore, by accessing different scale ranges, our method



Figure 7. **Samples from locally scaled ImageNet.** For each image, we show the target object at two different scales. Note that the scale of the background is always unchanged.

demonstrates the most consistent accuracy, reducing the std to 1.09 from 1.91. Additional ablations on DEC-related hyperparameters are provided in Sec. A5.2.

We also compare the time and memory requirements of DEC modules with differentiable optimization-based canonicalization, i.e., *Optim*. We train both methods with a batch size of 10 and image sizes of 224×224 . *Optim* takes 43.30 GB of GPU memory and spends 0.41s per iteration, while our DEC takes 5.75 GB and spends 0.19s. In other words, *Optim* requires more than 8 times the memory and twice the time than the DEC module. As discussed in Sec. 4.2, this makes it extremely difficult to apply *Optim* to deeper networks. We provide further discussion on runtime in Sec. A4.

5.3. Image Classification — ImageNet

Data setup. This experiment aims to benchmark local scale invariance in a more realistic real-world setting, where we create locally scaled images using ImageNet [17]. As shown in Fig. 7, only the target object in each image is scaled, while the background is kept the same.

In more detail, these images are created using the following procedure (see Fig. 4 for visualization): (a) We extract the bounding box of the target object by Grounding DINO [37] using the image labels. (b) With the bounding box, we extract a fine object mask using SAM [30] and (c) extract the object. (d) We inpaint the object mask region using LAMA [58]. (e) We scale the extracted object and (f) place the scaled object back onto the inpainted background. The object of interest is scaled by a factor within the range of [0.7, 1.3]. We fine-tune the pretrained models on a training dataset containing 10,000 images. We use 50,000 testing

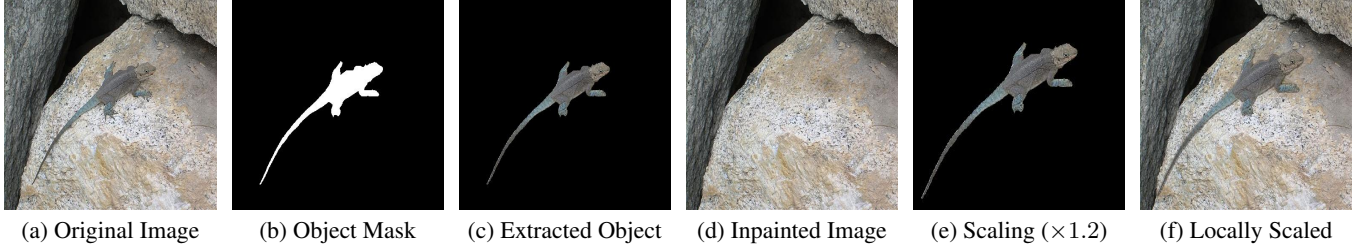


Table 4. **Generation procedure of locally scaled ImageNet.** Given (a) an image of a lizard, we first (b) obtain a mask of the lizard and (c) extract the lizard from the image. We then (d) inpaint the region without the lizard to get the background. Finally, (e) we scale the lizard by $1.2\times$ and (f) place it back onto the background to get the locally scaled image.

Method	ViT		DeiT		Swin		BEiT	
	Acc \uparrow	InvE \downarrow	Acc \uparrow	InvE \downarrow	Acc \uparrow	InvE \downarrow	Acc \uparrow	InvE \downarrow
<i>Base</i>	80.15	8.18	69.06	11.13	77.94	8.93	84.70	6.29
<i>Aug</i>	80.15	8.16	69.06	11.12	77.96	8.92	84.66	6.27
<i>Canon</i>	77.72	10.20	64.79	12.74	74.67	11.40	83.34	8.03
<i>InvL</i>	80.16	8.16	69.06	11.12	77.97	8.92	84.66	6.27
Ours	80.36	8.10	69.27	11.08	78.32	8.82	85.08	6.24

Table 5. **Results of local scale invariance on ImageNet.** For each method, we report the Top-1 Acc(%) and InvE(10^{-2}) across 4 architectures.

Method	Local Scales								Overall
	0.7	0.8	0.9	1.0	1.1	1.2	1.3		
<i>Base</i>	74.66	76.44	78.07	79.55	79.48	78.88	78.53	77.94 ± 1.65	
<i>Aug</i>	74.71	76.47	78.07	79.56	79.48	78.87	78.57	77.96 ± 1.64	
<i>Canon</i>	71.37	73.28	74.87	76.04	76.04	75.79	75.32	74.67 ± 1.61	
<i>InvL</i>	74.73	76.46	78.07	79.58	79.48	78.87	78.57	77.97 ± 1.64	
Ours	75.31	77.04	78.65	79.86	79.60	79.05	78.73	78.32 ± 1.49	

Table 6. **Per-scale results on ImageNet.** We report the Top-1 Acc(%) across various local scaling factors. Swin [38].

images for evaluation.

Baselines. For ImageNet, we use open-source models from Pytorch Image Models [64]. We fine-tune the pretrained weights using their training script, which we denote as *Base*. All other baselines are initialized from *Base*. We consider four different architectures ViT [18], DeiT [61], Swin [38], and BEiT [7]. During fine-tuning, all baselines follow the best practices of data augmentation and fine-tuning strategy for vision transformers [26, 38], including techniques such as label-smoothing, cutmix, etc.

Results. We present the ImageNet results in Tab. 5. We observe that our proposed DEC achieves the highest Acc with low InvE. Furthermore, we notice that the *Canon* is once again degrading the performance of the *Base* by distorting the input image. In Tab. 6, we report the performance of the baselines on Swin on different local scales. Our approach achieves the highest Acc on all local scales. Lastly, DEC produces the most consistent performance across different architectures, lowering the std of the Top-1 Acc to 1.49 from 1.65 of the *Base* model.

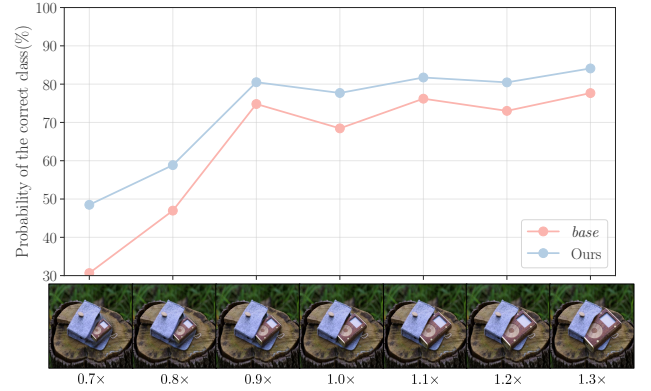


Figure 8. **Comparison on per-scale probability of correctness.** We locally scale the same input image within the range of $[0.7, 1.3]$ and report the probability of the correct class. Across all scales, our performance is 73.11 ± 0.13 while *Base*'s is 63.97 ± 0.17 .

We visualize DEC's consistency across multiple scales in Fig. 8. We show the probability of the correct class with the same image but locally scaled differently. We apply both methods to Swin [38]. Compared to *Base*, ours performs better on all scales and is more robust and invariant to challenging scenarios when the scale is extreme. In particular, when the input image is locally scaled by $0.7\times$, our method outperforms *Base* by 17.8%.

6. Conclusion

In this work, we introduce the Deep Equilibrium Canonicalizer (DEC) to improve the local scale consistency of deep networks, tackling the fundamental challenge of scale variation in computer vision. We demonstrate that DEC can be adapted into existing deep-net architectures to improve both performance and scale consistency. Extensive experiments on three datasets and six architectures demonstrate its effectiveness. Notably, on the ImageNet dataset, DEC further improves the pre-trained model's accuracy, even for the original unscaled images. Finally, we demonstrate the potential of DEQ as an effective canonicalizer for achieving equivariance and hope that this work inspires future DEC efforts toward other equivariances.

References

- [1] Edward H Adelson, Charles H Anderson, James R Bergen, Peter J Burt, and Joan M Ogden. Pyramid methods in image processing. *RCA engineer*, 1984. 1
- [2] Brandon Amos et al. Tutorial on amortized optimization. *Foundations and Trends® in Machine Learning*, 2023. 2, 4
- [3] Donald G. Anderson. Iterative procedures for nonlinear integral equations. *Journal of the ACM*, 1965. 5
- [4] Shaojie Bai, J Zico Kolter, and Vladlen Koltun. Deep equilibrium models. In *NeurIPS*, 2019. 2
- [5] Shaojie Bai, Vladlen Koltun, and J Zico Kolter. Multiscale deep equilibrium models. In *NeurIPS*, 2020. 2
- [6] Shaojie Bai, Zhengyang Geng, Yash Savani, and J Zico Kolter. Deep equilibrium optical flow estimation. In *CVPR*, 2022. 2
- [7] Hangbo Bao, Li Dong, and Furu Wei. BEiT: Bert pre-training of image transformers. In *ICLR*, 2022. 7, 8, 12
- [8] Axel Barroso-Laguna, Yurun Tian, and Krystian Mikolajczyk. Scalenet: A shallow architecture for scale estimation. In *Proceedings of the IEEE/CVF Conference on Computer Vision and Pattern Recognition*, pages 12808–12818, 2022. 2
- [9] Sourya Basu, Prasanna Sattigeri, Karthikeyan Natesan Ramamurthy, Vijil Chenthamarakshan, Kush R Varshney, Lav R Varshney, and Payel Das. Equi-tuning: Group equivariant fine-tuning of pretrained models. In *AAAI*, 2023. 2
- [10] Sourya Basu, Pulkit Katdare, Prasanna Sattigeri, Vijil Chenthamarakshan, Katherine Driggs-Campbell, Payel Das, and Lav R Varshney. Efficient equivariant transfer learning from pretrained models. In *NeurIPS*, 2024. 2
- [11] P. Burt and E. Adelson. The Laplacian pyramid as a compact image code. *IEEE Transactions on Communications*, 1983. 2
- [12] Peter J Burt and Edward H Adelson. The laplacian pyramid as a compact image code. In *Readings in computer vision*. 1987. 1
- [13] Gabriele Cesa, Leon Lang, and Maurice Weiler. A program to build E(N)-equivariant steerable CNNs. In *ICLR*, 2022. 2
- [14] Liang-Chieh Chen, George Papandreou, Iasonas Kokkinos, Kevin Murphy, and Alan L Yuille. Deeplab: Semantic image segmentation with deep convolutional nets, atrous convolution, and fully connected crfs. *IEEE TPAMI*, 2017. 1
- [15] Taco Cohen and Max Welling. Group equivariant convolutional networks. In *Proc. ICML*, 2016. 1, 2
- [16] Jifeng Dai, Haozhi Qi, Yuwen Xiong, Yi Li, Guodong Zhang, Han Hu, and Yichen Wei. Deformable convolutional networks. In *ICCV*, 2017. 2
- [17] Jia Deng, Wei Dong, Richard Socher, Li-Jia Li, Kai Li, and Li Fei-Fei. ImageNet: A large-scale hierarchical image database. In *CVPR*, 2009. 2, 5, 7
- [18] Alexey Dosovitskiy, Lucas Beyer, Alexander Kolesnikov, Dirk Weissenborn, Xiaohua Zhai, Thomas Unterthiner, Mostafa Dehghani, Matthias Minderer, Georg Heigold, Sylvain Gelly, et al. An image is worth 16x16 words: Transformers for image recognition at scale. In *ICLR*, 2021. 6, 7, 8, 12
- [19] Laura Downs, Anthony Francis, Nate Koenig, Brandon Kinman, Ryan Hickman, Krista Reymann, Thomas B McHugh, and Vincent Vanhoucke. Google scanned objects: A high-quality dataset of 3d scanned household items. In *ICRA*, 2022. 2, 5
- [20] Haoqi Fan, Bo Xiong, Karttikeya Mangalam, Yanghao Li, Zhicheng Yan, Jitendra Malik, and Christoph Feichtenhofer. Multiscale vision transformers. In *Proc. ICCV*, 2021. 1
- [21] K. Grauman and T. Darrell. The pyramid match kernel: discriminative classification with sets of image features. In *Proc. ICCV*, 2005. 1
- [22] Jiaqi Gu, Hyounjun Kwon, Dilin Wang, Wei Ye, Meng Li, Yu-Hsin Chen, Liangzhen Lai, Vikas Chandra, and David Z Pan. Multi-scale high-resolution vision transformer for semantic segmentation. In *CVPR*, 2022. 2, 7, 13, 14
- [23] Jason Hartford, Devon Graham, Kevin Leyton-Brown, and Siamak Ravanbakhsh. Deep models of interactions across sets. In *Proc. ICML*, 2018. 2
- [24] Kaiming He, Xiangyu Zhang, Shaoqing Ren, and Jian Sun. Spatial pyramid pooling in deep convolutional networks for visual recognition. *IEEE TPAMI*, 2015. 1
- [25] Kaiming He, Xiangyu Zhang, Shaoqing Ren, and Jian Sun. Deep residual learning for image recognition. In *CVPR*, 2016. 7, 12
- [26] Kaiming He, Xinlei Chen, Saining Xie, Yanghao Li, Piotr Dollár, and Ross Girshick. Masked autoencoders are scalable vision learners. In *CVPR*, 2022. 8, 12
- [27] Max Jaderberg, Karen Simonyan, Andrew Zisserman, et al. Spatial transformer networks. In *NeurIPS*, 2015. 2
- [28] Sékou-Oumar Kaba, Arnab Kumar Mondal, Yan Zhang, Yoshua Bengio, and Siamak Ravanbakhsh. Equivariance with learned canonicalization functions. In *ICML*, 2023. 3
- [29] Angjoo Kanazawa, Abhishek Sharma, and David Jacobs. Locally scale-invariant convolutional neural networks. *arXiv preprint arXiv:1412.5104*, 2014. 2, 6
- [30] Alexander Kirillov, Eric Mintun, Nikhila Ravi, Hanzi Mao, Chloe Rolland, Laura Gustafson, Tete Xiao, Spencer Whitehead, Alexander C Berg, Wan-Yen Lo, et al. Segment anything. In *ICCV*, 2023. 7
- [31] Svetlana Lazebnik, Cordelia Schmid, and Jean Ponce. Beyond bags of features: Spatial pyramid matching for recognizing natural scene categories. In *Proc. CVPR*, 2006. 1
- [32] Yann LeCun, Léon Bottou, Yoshua Bengio, and Patrick Haffner. Gradient-based learning applied to document recognition. *Proceedings of the IEEE*, 1998. 5
- [33] Jongmin Lee, Yoonwoo Jeong, and Minsu Cho. Self-supervised learning of image scale and orientation. *arXiv preprint arXiv:2206.07259*, 2022. 2
- [34] Tony Lindeberg. *Scale-space theory in computer vision*. 1993. 1
- [35] Iou-Jen Liu, Raymond A Yeh, and Alexander G Schwing. Pic: permutation invariant critic for multi-agent deep reinforcement learning. In *Proc. CORL*, 2020. 2
- [36] Iou-Jen Liu, Zhongzheng Ren, Raymond A Yeh, and Alexander G Schwing. Semantic tracklets: An object-centric representation for visual multi-agent reinforcement learning. In *Proc. IROS*, 2021. 2
- [37] Shilong Liu, Zhaoyang Zeng, Tianhe Ren, Feng Li, Hao Zhang, Jie Yang, Qing Jiang, Chunyuan Li, Jianwei Yang,

- Hang Su, et al. Grounding DINO: Marrying DINO with grounded pre-training for open-set object detection. In *ECCV*, 2024. 7
- [38] Ze Liu, Yutong Lin, Yue Cao, Han Hu, Yixuan Wei, Zheng Zhang, Stephen Lin, and Baining Guo. Swin transformer: Hierarchical vision transformer using shifted windows. In *ICCV*, 2021. 1, 6, 7, 8, 12
- [39] David G Lowe. Object recognition from local scale-invariant features. In *Proc. ICCV*, 1999. 1
- [40] David G Lowe. Distinctive image features from scale-invariant keypoints. *IJCV*, 2004. 1, 2
- [41] George Ma, Yifei Wang, Derek Lim, Stefanie Jegelka, and Yisen Wang. A canonicalization perspective on invariant and equivariant learning. In *NeurIPS*, 2024. 2, 3, 5
- [42] David Marr. *Vision: A computational investigation into the human representation and processing of visual information*. 1982. 1
- [43] Paul Micaelli, Arash Vahdat, Hongxu Yin, Jan Kautz, and Pavlo Molchanov. Recurrence without recurrence: Stable video landmark detection with deep equilibrium models. In *CVPR*, 2023. 2
- [44] Arnab Kumar Mondal, Siba Smarak Panigrahi, Oumar Kaba, Sai Rajeswar Mudumba, and Siamak Ravanbakhsh. Equivariant adaptation of large pretrained models. In *NeurIPS*, 2023. 1, 2, 3, 5
- [45] Maxime Oquab, Théo Darcet, Theo Moutakanni, Huy Vo, Marc Szafraniec, Vasil Khalidov, Pierre Fernandez, Daniel Haziza, Francisco Massa, Alaaeldin El-Nouby, et al. DINOv2: Learning robust visual features without supervision. *TMLR*, 2024. 6, 7, 12
- [46] Siba Smarak Panigrahi and Arnab Kumar Mondal. Improved canonicalization for model agnostic equivariance. In *CVPRW*, 2024. 1, 2, 3, 5
- [47] Omri Puny, Matan Atzmon, Heli Ben-Hamu, Ishan Misra, Aditya Grover, Edward J Smith, and Yaron Lipman. Frame averaging for invariant and equivariant network design. In *ICLR*, 2022. 2
- [48] Md Ashiqur Rahman and Raymond A Yeh. Truly scale-equivariant deep nets with Fourier layers. In *Proc. NeurIPS*, 2024. 1, 2, 6
- [49] Md Ashiqur Rahman and Raymond A. Yeh. Group down-sampling with equivariant anti-aliasing. In *The Thirteenth International Conference on Learning Representations*, 2025. 2
- [50] René Ranftl, Alexey Bochkovskiy, and Vladlen Koltun. Vision transformers for dense prediction. In *ICCV*, 2021. 12
- [51] Siamak Ravanbakhsh, Jeff Schneider, and Barnabas Poczos. Deep learning with sets and point clouds. In *Proc. ICLR workshop*, 2017. 2
- [52] Adria Recasens, Petr Kellnhofer, Simon Stent, Wojciech Matusik, and Antonio Torralba. Learning to zoom: a saliency-based sampling layer for neural networks. In *ECCV*, 2018. 2
- [53] Renan A Rojas-Gomez, Teck-Yian Lim, Alex Schwing, Minh Do, and Raymond A Yeh. Learnable polyphase sampling for shift invariant and equivariant convolutional networks. In *Proc. NeurIPS*, 2022. 2
- [54] Renan A Rojas-Gomez, Teck-Yian Lim, Minh N Do, and Raymond A Yeh. Making vision transformers truly shift-equivariant. In *CVPR*, 2024. 2
- [55] E.P. Simoncelli and W.T. Freeman. The steerable pyramid: a flexible architecture for multi-scale derivative computation. In *Proc. ICIP*, 1995. 1, 2
- [56] Ivan Sosnovik, Michał Szmaja, and Arnold Smeulders. Scale-equivariant steerable networks. In *ICLR*, 2020. 1, 2
- [57] Ivan Sosnovik, Artem Moskalev, and Arnold Smeulders. DISCO: accurate discrete scale convolutions. In *Proc. BMVC*, 2021. 1, 2, 6
- [58] Roman Suvorov, Elizaveta Logacheva, Anton Mashikhin, Anastasia Remizova, Arsenii Ashukha, Aleksei Silvestrov, Naejin Kong, Harshith Goka, Kiwoong Park, and Victor Lempitsky. Resolution-robust large mask inpainting with Fourier convolutions. In *WACV*, 2022. 7
- [59] Chittesh Thavamani, Mengtian Li, Nicolas Cebren, and Deva Ramanan. Fovea: Foveated image magnification for autonomous navigation. In *ICCV*, 2021. 2
- [60] Rui Tian, Zuxuan Wu, Qi Dai, Han Hu, Yu Qiao, and Yu-Gang Jiang. Resformer: Scaling vits with multi-resolution training. In *CVPR*, 2023. 2, 7, 13, 14
- [61] Hugo Touvron, Matthieu Cord, Matthijs Douze, Francisco Massa, Alexandre Sablayrolles, and Hervé Jégou. Training data-efficient image transformers & distillation through attention. In *ICML*, 2021. 7, 8, 12
- [62] Dimitri Van De Ville, Daniel Sage, Katarina Balać, and Michael Unser. The Marr wavelet pyramid and multiscale directional image analysis. In *European Signal Processing Conference*, 2008. 2
- [63] Maurice Weiler, Fred A Hamprecht, and Martin Storath. Learning steerable filters for rotation equivariant CNNs. In *Proc. CVPR*, 2018. 2
- [64] Ross Wightman. Pytorch image models. <https://github.com/huggingface/pytorch-image-models>, 2019. 8
- [65] Andrew Witkin, Demetri Terzopoulos, and Michael Kass. Signal matching through scale space. *International Journal of Computer Vision*, 1987. 1
- [66] Andrew P Witkin. Scale-space filtering. In *Readings in computer vision*. Elsevier, 1987. 2
- [67] Daniel Worrall and Max Welling. Deep scale-spaces: Equivariance over scale. In *Proc. NeurIPS*, 2019. 1, 2
- [68] Jin Xu, Hyunjik Kim, Thomas Rainforth, and Yee Teh. Group equivariant subsampling. In *Proc. NeurIPS*, 2021. 2
- [69] Yichong Xu, Tianjun Xiao, Jiaxing Zhang, Kuiyuan Yang, and Zheng Zhang. Scale-invariant convolutional neural networks. *arXiv preprint arXiv:1411.6369*, 2014. 2
- [70] Raymond A Yeh, Yuan-Ting Hu, and Alexander Schwing. Chirality nets for human pose regression. In *Proc. NeurIPS*, 2019. 2
- [71] Raymond A Yeh, Alexander G Schwing, Jonathan Huang, and Kevin Murphy. Diverse generation for multi-agent sports games. In *Proc. CVPR*, 2019. 2
- [72] Raymond A Yeh, Yuan-Ting Hu, Mark Hasegawa-Johnson, and Alexander Schwing. Equivariance discovery by learned parameter-sharing. In *Proc. AISTATS*, 2022. 2

- [73] Greg Zaal. Hdri haven: Free high-quality hdr images under a cc0 license, 2020. Accessed via Poly Haven (formerly HDRI Haven). [5](#)
- [74] Manzil Zaheer, Satwik Kottur, Siamak Ravanbakhsh, Barnabas Poczos, Ruslan R Salakhutdinov, and Alexander J Smola. Deep sets. In *Proc. NeurIPS*, 2017. [2](#)
- [75] Richard Zhang. Making convolutional networks shift-invariant again. In *Proc. ICML*, 2019. [2](#)
- [76] Hengshuang Zhao, Jianping Shi, Xiaojuan Qi, Xiaogang Wang, and Jiaya Jia. Pyramid scene parsing network. In *Proc. CVPR*, 2017. [1](#)

Appendix

The appendix is organized as follows:

- In Sec. A1, we provide additional implementation details of our method.
- In Sec. A2, we provide additional details of our monotone scaling group and its parameterization.
- In Sec. A3, we provide the detailed proofs for our lemmas in Sec. A4, we discuss the runtime of the DEC module.
- In Sec. A5, we provide additional analysis and results.

A1. Implementation details

DEC module. For all experiments, we model the DEC module as 2 layered CNN mapping with 64 and 128 channels. We perform adaptive pooling at the end to get the desired number of monotone scaling parameters.

Vanilla Canonicalization. To train vanilla canonicalization, we discretized the monotone scale parameter into 64 different configurations for the locally scaled MNIST and object segmentation and 25 different configurations for locally scaled ImageNet. The learnable energy functions are implemented via a 3 layer CNN.

Locally Scaled Object Segmentation. The pretrained models ViT [18], Swin [38], and DINOv2 [45] are finetuned on the training set for 120 epochs. We set the initial learning rate at $1e-4$ and scaled it by a factor of 0.7 for each 30 epoch. We use DPT [50] style segmentation head. We use the per-pixel cross-entropy loss to train each model. We set the weight for the “background” pixel class to 0.1, and the weights of all other object classes are set to 1. All baselines are finetuned for 60 epochs with an initial learning rate of $2e-5$.

Locally Scaled MNIST. Each architecture is trained for 50 epochs. We set the initial learning rate at $1e-4$ for ResNet [25], ViT [18], DeiT [61], and BEiT [7]; $2e-5$ for DINOv2 [45]; and $8e-4$ for Swin [38]. All baselines are fine-tuned for 40 epochs.

Locally Scaled ImageNet. All baselines are fine-tuned following standard data augmentation practice for ImageNet finetuning [26, 38]. We use a batch size of 80 and an initial learning rate of $1e-7$ with 5 warm-up epochs. We list common training hyperparameters in Tab. A1.

A2. Monotone scaling group

A2.1. Group axioms

Our monotone scaling set L must meet the following axioms to be considered as a group. Here, “ \cdot ” represents the group product described in Eq. (9). The 4 axioms are as follows:

- **Closure:** $\forall a, b \in L, a \cdot b \in L$
- **Associativity:** $\forall a, b, c \in L, a \cdot (b \cdot c) = (a \cdot b) \cdot c$
- **Existence of Identity:** $\exists e \in L : \forall a \in L, e \cdot a = a$

Hyperparameter	Value
Scheduler	Cosine
Weight decay	0.05
Warmup epochs	5
Mixup Alpha	0.8
Label smoothing	0.1
Random Erase Prob	0.25
Layer Decay Factor	0.75
Epochs	20

Table A1. ImageNet Finetuning Parameters

- **Existence of Inverse:** $\forall a \in L, \exists a^{-1} \in L : a \cdot a^{-1} = e$.

A2.2. 2D Monotone scaling group

Construction of monotone scaling group in 2D. To form the monotone scaling group on $2D$, the set

$$L_{2D} : \{l : [0, 1]^2 \rightarrow [0, 1]^2\}$$

should satisfy the two following properties:

- For all $x \in [0, 1]^2$ there is a neighborhood $\mathcal{W} \subset [0, 1]^2$ such that any function $l \in L_{2D}$ can be approximated by a linear function with Jacobian $J_l(x) \in \text{SPD}(2)$, i.e., 2×2 symmetric positive definite Jacobian. This condition imposes local monotonicity on l .
- For all $l_1, l_2 \in L_{2D}$, their local Jacobian $J_{l_1}(x_1)$ and $J_{l_2}(x_2)$ commutes for $x_1, x_2 \in [0, 1]^2$.

Formally, we state this in Lemma 2.

Lemma 2. *The set of all locally monotone increasing functions L_{2D} with commutative Jacobian is a valid group under the binary operation of function composition.*

Proof. We provide the detailed proof in Sec. A3.2. \square

Parametrization of l . We parameterize l through a set of independent monotone functions along the x and y axes via bilinear interpolation. Specifically, we decompose the function l into two functions as

$$l(x, y) = (l_X(x, y), l_Y(x, y)), \quad (\text{A26})$$

where $l_X, l_Y : [0, 1]^2 \rightarrow [0, 1]$. We parameterize each of them as piecewise linear functions. To achieve this we discretize the domain $[0, 1]^2$ into uniform grid $\mathcal{G} = \mathcal{X} \times \mathcal{Y}$ where $\mathcal{X} = \{x_0 = 0, x_1, \dots, x_N = 1\}$ and $\mathcal{Y} = \{y_0 = 0, y_1, \dots, y_M = 1\}$. We assume the set is ordered, i.e., $x_i < x_j$ when $i < j$.

We define independent monotone functions along each row y_j and each column x_i of the grid \mathcal{G} as follows:

For $x \in [x_{n-1}, x_n]$, the monotone function along row y_j is given by:

$$l^{y_j}(x) = \phi_{x_{n-1}}^{y_j} + \frac{\phi_{x_n}^{y_j} - \phi_{x_{n-1}}^{y_j}}{x_n - x_{n-1}} \times (x - x_{n-1}). \quad (\text{A27})$$

Similarly, for $y \in [y_{m-1}, y_m)$, the monotone function along column x_i is given by:

$$l^{x_i}(y) = \phi_{y_{m-1}}^{x_i} + \frac{\phi_{y_m}^{x_i} - \phi_{y_{m-1}}^{x_i}}{y_m - y_{m-1}} \times (y - y_{m-1}) \quad (\text{A28})$$

Here, ϕ s are the learnable parameters and to preserve monotonicity we impose restriction $\phi_{x_{n-1}}^{y_j} \leq \phi_{x_n}^{y_j} \forall j, n$ and $\phi_{y_{m-1}}^{x_i} \leq \phi_{y_m}^{x_i} \forall i, m$.

Finally, we obtain $l_X(x, y)$ from l^{y_i} s via linear interpolation as

$$l_X(x, y) = l^{y_{j-1}}(x) + \frac{l^{y_j}(x) - l^{y_{j-1}}(x)}{y - y_{j-1}} \quad (\text{A29})$$

when $y \in [y_{j-1}, y_j)$. We defined $l_Y(x, y)$ similarly. We approximate the inverse function l^{-1} by computing the inverses of each l^{x_i} and l^{y_j} individually.

A3. Complete Proofs of Lemmas and Claims

A3.1. Proof of Lemma 1

Lemma 1. *The set of all continuous strictly monotonic increasing functions L is a group under the binary operation of function composition.*

Proof. To prove that the set of all continuous strictly monotonic increasing functions L forms a group under function composition, we need to verify four properties: closure, associativity, identity element, and inverse element.

Closure. Let $l_1, l_2 \in L$. Since l_1 and l_2 are continuous and strictly increasing, for any $x_1, x_2 \in [0, 1]$ if $x_1 < x_2$, then $l_1(x_1) < l_1(x_2)$. Thus, $l_2(l_1(x_1)) < l_2(l_1(x_2))$, showing that $l_1 \circ l_2$ is strictly increasing. Moreover, $l_1 \circ l_2$ is continuous because both are continuous.

Associativity. Function composition is inherently associative, thus satisfying the property.

Identity Element. The identity function is continuous and strictly increasing, so also an element of L .

Inverse Element. Strictly monotone functions have an inverse, and the inverse is also monotonic. Thus, the inverse is also an element of L .

Therefore, we conclude that L is a group. \square

A3.2. Proof of Lemma 2

Lemma 2. *The set of all locally monotone increasing functions L_{2D} with commutative Jacobian is a valid group under the binary operation of function composition.*

Proof. To verify that L_{2D} forms a group, we check the following properties:

Closure: For any $l_1, l_2 \in L_{2D}$, their composition $l_1 \circ l_2$ is also a locally monotone-invertible function.

Because the local Jacobian of the composition $l_1 \circ l_2$ is

$$J_{l_1 \circ l_2}(x) = J_{l_1}(l_2(x)) \cdot J_{l_2}(x) \quad \forall x \in [0, 1]^2. \quad (\text{A30})$$

Since $J_{l_1}, J_{l_2} \in \text{SPD}(2)$ and commutes, their product $J_{l_1} \cdot J_{l_2}$ is also a SPD matrix. The composition of invertible functions is also invertible. And the $J_{l_1 \circ l_2}$ commutes due to associativity of matrix product. Thus $l_1 \circ l_2 \in L_{2D}$.

Associativity: Function composition is inherently associative, i.e., for all $l_1, l_2, l_3 \in L_{2D}$, we have

$$(l_1 \circ l_2) \circ l_3 = l_1 \circ (l_2 \circ l_3). \quad (\text{A31})$$

Existence of Identity: The identity function l has 2×2 identity matrix as local Jacobian. Thus, it maintains all the conditions of L_{2D} .

Existence of Inverse: The inverse function of any $l \in L_{2D}$ can be obtained by inverting the local Jacobians. Specifically, for any $l \in L_{2D}$, the inverse l^{-1} exists and satisfies:

$$J_{l^{-1}}(x) = J_l(l^{-1}(x))^{-1} \in \text{SPD}(2) \quad \forall x \in [0, 1]^2 \quad (\text{A32})$$

Furthermore, $J_{l^{-1}} J_{l_k} = J_{l_k} J_{l^{-1}}$ for any $l_k \in L_{2D}$ as

$$J_l J_{l_k} = J_{l_k} J_l \quad (\text{A33})$$

$$\Rightarrow J_l^{-1}(J_l J_{l_k}) = J_l^{-1}(J_{l_k} J_l), \text{ (left multiply by } J_l^{-1}) \quad (\text{A34})$$

$$\Rightarrow J_{l_k} = J_l^{-1} J_{l_k} J_l \quad (\text{A35})$$

$$\Rightarrow J_{l_k} J_l^{-1} = J_l^{-1} J_{l_k} \text{ (right multiply by } J_l^{-1}). \quad (\text{A36})$$

Thus, $l^{-1} \in L_{2D}$.

Therefore, L_{2D} satisfies all group axioms, completing the proof. \square

A4. Runtime of the DEC Module

We use Anderson Acceleration to approximate the fixed point of the DEC. This requires a fixed number of forward passes through the lightweight DEC module. The computational complexity of this iterative process is $\mathcal{O}(jT_{\text{DEC}})$, where j is a fixed number of required iterations and T_{DEC} is the computation cost associated with a single forward pass of the DEC module. The hyperparameter j governs the trade-off between computational cost and the accuracy of the fixed-point approximation.

Empirically, for DINO-v2, the DEC module requires 24% (0.16 sec) of the total required time (0.66 sec) to process a batch of 128 images of size 224×224 .

A5. Additional Results

A5.1. Additional Baselines

To evaluate the effectiveness of the DEC module in models with handcrafted hierarchical feature processing or image pyramid structures, we adapt our approach to HRViT [22] and ResFormer [60] and report the results in Tab. A2.

Method	HRVit [22]	Resformer [60]
<i>Aug</i>	93.22	91.04
<i>Canon</i>	94.93	95.27
<i>InvL</i>	95.91	94.92
Ours	96.67	96.91

Table A2. Hierarchical baselines on scale-MNIST

		# layers in DEC Mod.			
		1	2	3	4
# DEC Mod	1	93.59	94.47	94.04	93.22
	2	94.98	96.04	95.16	95.25
	3	96.66	96.17	96.67	96.38
	4	96.58	96.78	96.65	96.50

Table A3. Ablation on the number of DEC modules and layers per module on scale-MNIST

		Multiples (\times) of grid			
		1.0	1.5	2.0	2.5
layers	2	96.61	96.95	97.06	97.94
	3	96.62	96.91	97.08	97.08

Table A4. Acc. at multiple of initial grid size of 4 with varying number of layers in DEC on scale-MNIST.

Methods	ViT	DeiT	Swin	BEiT
<i>Base</i>	81.29	70.67	79.55	85.79
<i>Aug</i>	81.29	70.70	79.56	85.66
<i>Canon</i>	79.23	66.92	76.04	84.29
<i>InvL</i>	81.29	70.71	79.58	85.66
Ours	81.43	70.92	79.86	86.04

Table A5. Acc. on unmodified (scale-1) ImageNet images.

that the DEC module has learned to stretch/squeeze regions of the digits. However, the exact reasoning on why such scaling is beneficial to the deep-net remains challenging. The interpretability of the choice of learned canonical elements in a group is largely underexplored in the literature.

A5.2. Additional Ablation Study

We perform additional ablation studies on the scale-MNIST dataset to evaluate the effect of (i) the number of DEC modules and (ii) the number of layers within each DEC module. The results are summarized in Tab. A3. We observe that increasing the number of DEC modules, *i.e.*, repeatedly canonicalizing features throughout the network, improves performance compared to applying canonicalization only at the input level.

We provide an additional ablation study on the choice of grid size for local scaling and report the results in Tab. A4. We observe that increasing the grid size improves the performance as it allows more flexible spatial parameterization of the local scaling operations.

To assess potential side effects of scale equivariance, we report the accuracies of the adapted models on images of scale 1, *i.e.*, unmodified images in Tab. A5. We do not observe any drop in the performance.

A5.3. Additional Visualizations

Following the settings of Fig. 8, we report the results for more input images in Fig. A1. We observe that Ours is consistently better and more robust on all scales in comparison to *Base*; especially on the more extreme local scale factors.

We present visualizations of learned monotone scaling by the DEC trained on MNIST in Fig. A2. We observe

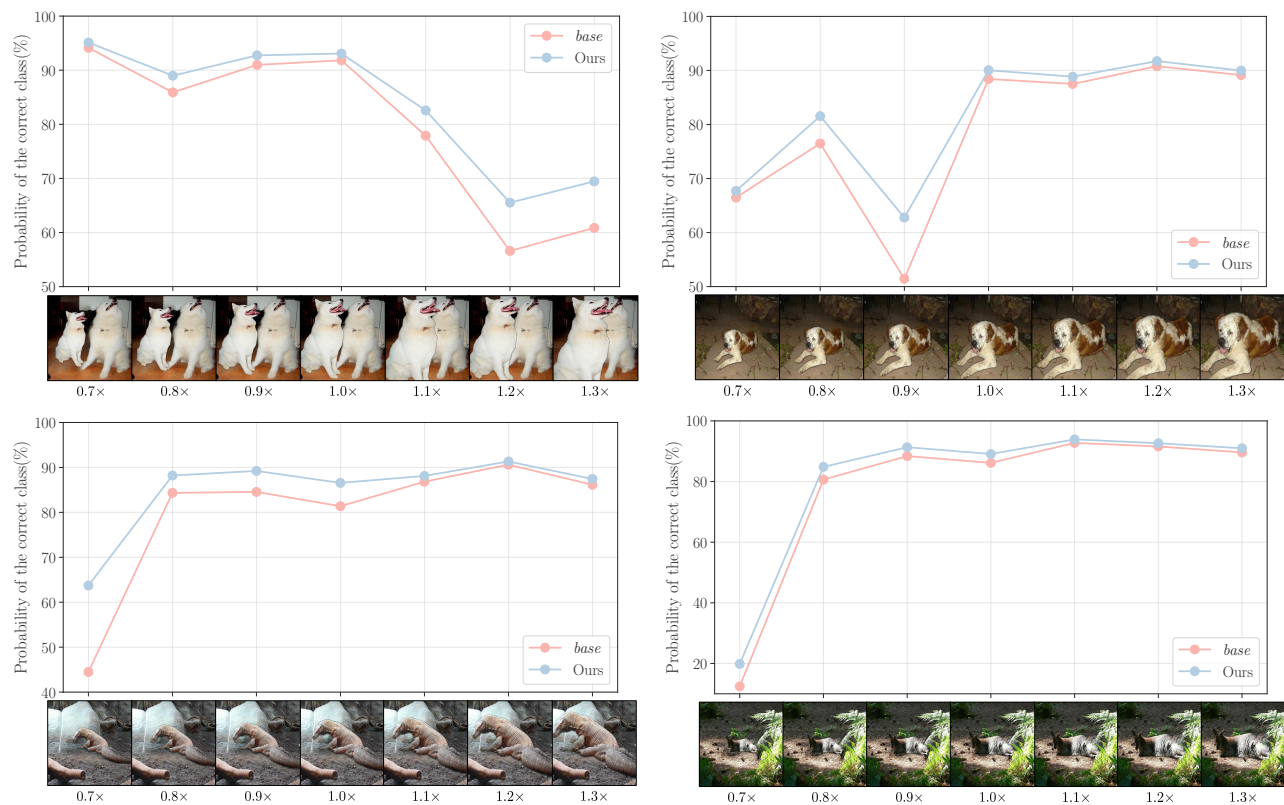


Figure A1. **Comparison on per-scale probability of correctness.** We locally scale the same input image within the range of $[0.7, 1.3]$ and report the probability of the correct class.

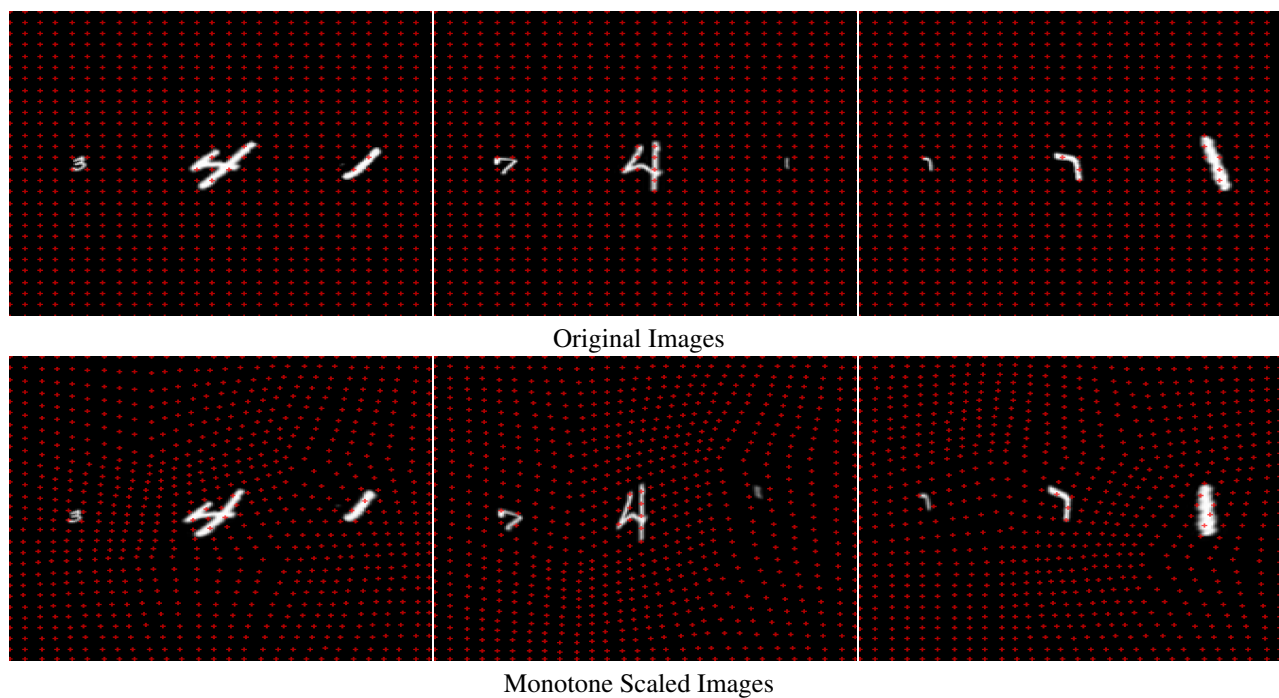


Figure A2. **Learned monotone scaling on locally scaled MNIST.** We observe that stretching/squeezing is performed on the area with digits.